Advances in Cancer Biology - Metastasis 7 (2023) 100089

Contents lists available at ScienceDirect

Advances in Cancer Biology - Metastasis

journal homepage: www.journals.elsevier.com/advances-in-cancer-biology-metastasis

Alpha mangostin inhibits proliferation, migration, and invasion of human breast cancer cells via STAT3 inhibition

Lakshmi Vineela Nalla [a,b], Anil Dharavath [a], Santosh Kumar Behera [c], Amit Khairnar [a,d,e,*]

[a] Department of Pharmacology and Toxicology, National Institute of Pharmaceutical Education and Research (NIPER), Ahmedabad, Gujarat, India
[b] K L College of Pharmacy, Koneru Lakshmaiah Education Foundation, Green Fields, Vaddeswaram, Guntur, Andhra Pradesh, India
[c] Department of Biotechnology, National Institute of Pharmaceutical Education and Research (NIPER) – Ahmedabad, Palaj, Gandhinagar, 382355, Gujarat, India
[d] International Clinical Research Center (ICRC), St. Anne's University Hospital, Brno, Czech Republic
[e] Department of Physiology, Masaryk University, Kamenice 753/5, 625 00 Brno, Czech Republic

ARTICLE INFO

Keywords:
STAT3
PKM2
α-M
Breast cancer
Migration
And hnRNP-A1

ABSTRACT

Background: Signal Transducer and Activator of Transcription 3 (STAT3) is an identified critical protein associated with the progression of cancer. Alpha mangostin (α-M), a powerful dietary xanthone found to have anti-cancer properties against various cancers. However, the precise mechanism of its anti-cancer activity is not fully understood. Therefore, the current work hypothesized that targeting STAT3 with α-M inhibits the migration, invasion, and proliferation of breast cancer cells. Firstly, we evaluated the binding affinity of α-M/STAT3 complex using molecular dynamic simulations (MDS) and further we determined the likely underlying mechanism of STAT3 through *in-vitro* experiments. α-M treatment affected the levels of STAT3 phosphorylation, hnRNP-A1, PKM2, and EMT markers. α-M stimulation in breast cancer cells also resulted in suppressed migratory and invasive behaviour. More importantly, the treatment also affected the Ki67 and BrdU positive cells. In summary, we found the anti-migratory and anti-proliferative actions of α-M in breast cancer cells via STAT3 inhibition. Also, the study significantly adds a new nutraceutical for therapeutic intervention of invasive breast cancer.

1. Introduction

Dietary functional compounds known as nutraceuticals receives a huge interest in the scientific community to address the inadequacies of traditional medicine. Owing to the anti-cancer potential, their frequent consumption can also lower the risk of multiple cancer types, providing an alternative approach to treat and manage cancer. Epidemiological studies also reveal an inverse link between the consumption of phytochemicals and the risk of breast cancer [1]. Breast cancer is the world's second most deadly cancer, with 1 in every 8 women getting metastases. Despite the fact that treatment of benign tumor patients achieves a 5-year survival rate of 99%, the incidence and death rates continue to rise [2–4]. As a result, novel therapeutics in treating cancer progression are required to extend patients' survival and to provide quality life.

STATs are a group of transcription factors that have a critical role in physiological functions. STAT3 is one of the essential STAT proteins in the development of breast cancer [5,6]. Constitutive activation of STAT3 in response to oncogenic events results in the dysregulation of breast carcinomas [7]. Activation of STAT3 triggers downstream pathways implicated in cell cycle regulation (Cyclin D1 and c-Myc) [8], apoptosis inhibition (Mcl-1, Bcl-xL, and survivin) [9], angiogenesis induction (VEGF), and Warburg effect (HK2, hnRNPA1 and PKM2) [10]. *In-vitro* and *in-vivo* research supports pY705 modification on STAT3 requirement for tumor growth, autophagy and metastasis [11], and recommends STAT3 as a validated target for cancer treatment. Furthermore, clinical trials using STAT3 inhibitors (OPB-51602) show promising results in malignant conditions [12]. As a result, there is a need to investigate natural compounds that can inhibit STAT3 phosphorylation to target cancer progression with minimal side effects.

α-M, a highly abundant dietary xanthone isolated from the pericarp of Garcinia Mangostana Linn., sparked a considerable interest in South East Asian medical uses. A substantial body of data supports the use of a natural product to treat advanced cancer patients. Several studies assesses the anti-cancer, anti-inflammatory, and anti-apoptotic effects of α-M in various disorders [13,14]. Further, α-M was found to inhibit fatty acid synthesis [15] and cancer stemness [16] in breast cancer. In addition, α-M had anti-metastatic activity against several cancers [17–19].

* Corresponding author. National Institute of Pharmaceutical Education and Research (NIPER), Ahmedabad, Palaj, Gandhinagar, 382355, Gujarat, India.
E-mail addresses: amitk@niperahm.res.in, amitkhairnar520@gmail.com (A. Khairnar).

https://doi.org/10.1016/j.adcanc.2023.100089
Received 8 June 2022; Accepted 13 January 2023
Available online 14 January 2023

Abbreviations

CASTp	Computed Atlas of Surface Topography of proteins
ChIP	Chromatin Immunoprecipitation
GAPDH	Glyceraldehyde 3-phosphate dehydrogenase
GLIDE	Grid-based Ligand Docking with Energetics
hnRNP-A1	Heterogeneous nuclear ribonucleoprotein-A1
hnRNP-A2	Heterogeneous nuclear ribonucleoprotein-A2
LDH	Lactate dehydrogenase
PKM1	Pyruvate Kinase M1
PKM2	Pyruvate Kinase M2
miRNA	Micro Ribonucleic Acid
MMP2	Matrix metalloproteinase-2
PTB	Polypyrimidine tract-binding
STAT3	Signal transducer and activator of transcription 3

For example, α-M inhibits STAT3 in gastric cancer [10], MEK/ERK [20], JNK signaling [21], PI3K/AKT [22] to modulate metastasis. The hnRNPA-1/PKM2 axis has a significant role in regulating cell proliferation and metastasis [23], glucose metabolism [10], and the Warburg effect [24]. Therefore, addressing the hnRNPA-1/PKM2 pathway may have an effect on the aforementioned processes. The impact of α-M on breast cancer invasiveness via STAT3 inhibition is unclear. Owing to the above stated functions of α-M, in the current study we investigated the binding ability between STAT3/α-M complex using MDS and subsequently analyzed the impact of α-M on migration, invasion, and proliferation of breast cancer cells in relation to STAT3. We hypothesize that α-M treatment would limit proliferation, migration and invasion of human breast cancer cells.

2. Materials and methods

2.1. In-silico study

2.1.1. Sequence, structure and functional analysis of STAT3 protein

STAT3 structure, sequence, and functional information were obtained from UniProtKB - P40763 (STAT3 HUMAN). The length of STAT3 was 552 (136–687) amino acids. The X-ray diffraction structure of STAT3 with PDB ID: 6NJS and resolution of 2.70 was obtained from the PDB database. The co-crystallized compounds were taken from BIOVIA Discovery Studio 4.5 Visualiser (BIOVIA, San Diego, CA, USA).

2.1.1.1. Structure refinement of STAT3. The experimental structure of STAT3 acquired from the PDB was discovered to have numerous missing residues, rendering the 3D structure incomplete. The Protein Preparation wizard in Schrodinger Maestro v2021.1 was used to fill in the missing STAT3 residues.

2.1.1.2. Retrieval of drug/compound. The structural information for α-M and STX-0119 (Standard STAT3 inhibitor) was obtained in Structure Data Format from PubChem using compound IDs 5281650 and 4253236. The obtained structures were saved in. pdb format.

2.1.1.3. Prediction of binding site. The STAT3 binding site was predicted using the consensus results of the online servers such as Computed Atlas of Surface Topography of Proteins (CASTp), GHECOM (https://pdbj.org/ghecom/), DEPTH (http://cospi.iiserpune.ac.in/depth), and PDBsum, which depicted the active site residues involved in binding site formation.

2.1.2. Molecular docking studies

Glide (Grid-based Ligand Docking with Energetics), Schrödinger, LLC, New York, NY, 2021 [25] was utilized in extra precision (XP) mode for docking α-M and STX-0119 (standard) against STAT3 protein [26]. Based on binding energy values, intermolecular hydrogen (H)-bonds, and other hydrophobic and electrostatic interactions, the best-docked complexes were described and processed for further computational study. To demonstrate the existence of intermolecular links between protein-drug complexes, LigPlot+ (https://www.ebi.ac.uk/thornton-srv/software/LigPlus/) was employed.

2.1.3. Molecular dynamics (MD) simulations

MD is a sophisticated computational method for predicting and analyzing the physical motions of atoms and molecules in the context of macromolecular structure-to-function interactions [27]. The atoms and molecules are allowed to interact for a predetermined time, demonstrating the system's dynamic "evolution" [28]. We utilized the Desmond programme to perform MD simulations of the STAT3/α-M and STAT3/STX-0119 complexes to confirm ligand binding modalities and comprehensively view the protein-ligand complexes. A 100 ns MD simulation was performed on the top-scoring ligand-protein complexes. Minimization, heating, equilibration, and production run were all part of the MD process [29]. The protein-ligand complexes were minimized using the OPLS4 force field, and topology and atomic coordinates were produced automatically [30]. The chemical was then submerged in an SPC solvent model orthorhombic box. The physiological pH was neutralized by adding 0.15 M NaCl. The water box was created using the Particle Mesh Ewald (PME) boundary condition to guarantee that no solute atoms occurred within 10 distance of the border. The NPT ensemble was used to model the complete system at 300 K for 100 ns, and the structural modifications and dynamic behaviour of the protein were studied using RMSD and RMSF graphs. The difference between a protein's backbones from its initial structural conformation to its final location is calculated using root mean square deviation (RMSD). The RMSF approach is used to identify a protein's or complex flexible region [31]. The simulated interaction diagram displays the most likely ligand binding mode at the binding site of the enzyme [32].

2.2. In-vitro study

2.2.1. Cell lines and reagents

α-M was isolated as previously published [33]. MCF-10A (normal human mammary epithelial cells), MCF-7 and MDA-MB-231 (human breast cancer cells) cell lines were procured from American Type Culture Collection (ATCC; Rockville, MD, USA). The following requirements were used for conducting the experiments; DMEM + F12 with supplements, DMEM-High glucose, Leibovitz's L-15, Fetal Bovine Serum (FBS), Penicillin-streptomycin, and Trypsin-EDTA from Gibco, Life Technologies, Resazurin (Sigma, R7017), DAPI (Sigma, D9542), BrdU (Sigma, B5002), TRIzol reagent (Thermo Fisher Scientific), iScript cDNA synthesis kit (Bio-rad). KiCqStart primers of hnRNPA1 and 18S rRNA primers were procured from Sigma. Antibodies namely STAT3 (ab119352), pSTAT3 (ab76315), E-cadherin (ab76055), MMP-2 (ab37150), β-actin (ab6276), Ki67 (ab16667), BrdU (B8434), and PKM2 antibody (CST, #4053) were used for the experiments.

2.2.2. Cell culture and maintenance

MCF-7 and MDA-MB-231 cells were cultured in DMEM-high glucose, and Leibovitz's L-15 media respectively, supplemented each with 10% FBS and penicillin 100 units/ml and streptomycin 100 units/mL. MCF-7 cells were cultured at 37 °C in a humidified atmosphere with 5% CO_2 whereas MDA-MB-231 cells were cultured at 37 °C in a humidified atmosphere without CO_2. Cells were harvested with trypsin-EDTA upon reaching their exponential growth phase. The media was changed weekly thrice. The cell lines with a passage number of less than 15 was maintained throughout all experiments.

2.2.3. Cell viability assay

The cellular metabolism was evaluated by using Resazurin assay, also known as Alamar blue assay. In brief, MCF-7 and MDA-MB-231 cells were harvested using trypsin-EDTA, counted and seeded at a concentration of 1×10^4 cells/well into a 96-well plate. The plate was incubated overnight for cell attachment. Media was removed on the following day; cells were exposed to different concentrations of α-M ranging from 0.5 to 5 μM. After the 24 h treatment period, existing media with the drug was removed, and freshly prepared resazurin solution was added to the plate and further incubated for 3–4 h. Cellular viability was measured by taking the readings at 560 nm and 590 nm wavelength using a Varioskan Lux multi-mode spectrophotometer (Thermo). Data was acquired with SkanIt software (generation 4) and analyzed for % cell viability. The experiment was repeated in triplicate at three different times.

$$\% \text{ Cell Viability} = (\text{Mean absorbance of treatment group} / \text{Mean absorbance of control}) \times 100$$

2.2.4. Western blotting

Sample preparation and execution of the experiment was in accordance with the published paper [33]. In brief, cells were lysed using RIPA buffer, and the total protein quantification was performed using BCA (Bicinchoninic acid) reagent. Samples (20 μg protein + Laemmli buffer) were loaded, resolved in the gel, and transferred to the PVDF membrane. Subsequently, membranes were subjected for blocking followed by the incubation with primary antibodies-mouse, anti-STAT3 (1:5000), rabbit anti-pSTAT3 Y705 (1:10,000), rabbit anti-E-cadherin (1:500), rabbit anti-MMP2 (1:2000), mouse anti-β-actin (1:10,000), and rabbit anti-PKM2 (1:1000) overnight at 4 °C followed by secondary antibody (ab6789, Goat anti-mouse IgG-HRP,1:10,000 and ab6721, Goat anti-rabbit IgG-HRP, 1:10,000) incubation. Antigen-primary-secondary complexes were visualized and analyzed.

2.2.5. RNA isolation and analysis by RT-PCR

RNA isolation and experiment was conducted as per the published paper [34]. In brief, RNA was isolated, and RNA purity was quantified using Nanodrop spectrophotometer 2000C (Thermo scientific). The samples having the 260/280 ratio in the range of 1.9–2.1 were subjected for cDNA synthesis using 1 μg of isolated RNA with a cDNA kit (Bio--Rad). Real-time PCR was performed by means of iTaq SYBR green and primers (18S and hnRNPA1) to calculate $2^{-(\Delta\Delta Ct)}$ with the help of the Real-Time PCR instrument (Bio-Rad CFX96). Primer sequences were provided in the Supplementary Table S1.

2.2.6. Wound healing assay

A wound-healing assay was performed to evaluate the effect of α-M on the migration of cells. In brief, breast cancer cells were seeded and maintained in a 12-well plate until they were fully confluent. Later, they were serum-starved overnight. On the next day, media was removed, and the wound was created with a 10 μL micro-tip followed by PBS washing to remove the uneven edges of the wound. Subsequently, cells were exposed to different concentrations of α-M with a low concentration of serum (1%) [35]. Perpendicular lines were drawn with respect to the wound, and images were acquired within the area marked by the vertical lines on the wound using an inverted microscope (Zeiss, USA). The wound area of the images acquired at different time points (0, 12, and 24 h) was quantified using ImageJ [36].

2.2.7. Invasion assay

For conducting the invasion assay, the cells were serum-starved overnight before experimentation. On the next day, 5×10^4 cells were seeded into the matrigel coated transwell with serum-free media containing treatment. In the lower chamber, media containing 10% FBS was added and incubated at 37 °C for 24 h. After the treatment period, the transwell inserts were subjected to 4% PFA fixation (10min, RT) followed by methanol permeabilization (15min, RT). Subsequently, the inserts were stained with 0.1% crystal violet for 15min, RT. The non-invaded cells were removed using cotton swabs, and membranes were mounted and counted for invaded cells using ImageJ [36].

2.2.8. Immunofluorescence

For immunocytochemistry, 3×10^4 cells were seeded into the Millicell EZ SLIDE, 8-well chambered, sterile (Merck, Millipore). The next day, the MCF-7 and MDA-MB-231 cells were treated with α-M at respective concentrations. After the treatment period, the cells were fixed (4% PFA), permeabilized (0.1% Triton-X) and blocked (1% BSA) at RT. The cells were incubated with the rabbit anti-Ki67 primary antibody (ab16667, 1:250) overnight. The next day, the samples were subjected to secondary antibody goat anti-rabbit (1:500) for 1 h. Further, the cells were counterstained with DAPI (1 μg/ml) for 3 min, RT. The samples were washed, mounted and the images were acquired using a confocal microscope (Leica) at 40X with zoom factor-2.

2.2.9. BrdU assay

For conducting BrdU assay, 3×10^4 cells were seeded into the Millicell EZ SLIDE, 8-well chambered, sterile (Merck, Millipore). The cells were treated for 24 h with the respective concentrations of α-M. After the treatment period, the cells were further incubated for 24 h with BrdU (10 μM). Then the cells were fixed with 70% ethanol for 10min, followed by denaturation (2 M HCl, 30min, RT) and neutralisation (0.1 M sodium borate buffer, pH-8.5, 10min, RT). After washing with 1x PBS 3 times, the cells were blocked (1% BSA, 1 h) and incubated with mouse anti-BrdU antibody (Sigma-B8434, 1–2 μg/ml) overnight. On a subsequent day, washing was followed by secondary antibody incubation. The cells were counterstained using DAPI and mounted. The images were captured at 40X with zoom factor-2 using Leica confocal microscope [37].

2.2.10. Statistical analysis

Data was expressed as mean ± SEM. Statistical data analysis of different groups was executed using one way ANOVA and Tukey's multiple comparisons post-hoc test by GraphPad Prism Version 5.01. $p < 0.05$ was considered as statistically significant.

3. Results

3.1. In-silico study

3.1.1. Molecular docking

The consensus results of all the three web servers depicted the residues Leu666, Glu638, Trp623, Lys658, Tyr657, Gly656, Ile653, and Met660 that take part in active site formation. The binding energy of STAT3/α-M and STAT3/STX-0119 (standard) interactions complexes are presented in Table 1 and Fig. S1 (a, b). The docking data indicated

Table 1
Molecular docking score of α-M and STX-0119 against STAT3 protein.

Target	PubChem CID	Drug	Binding Energy (kcal/mol)	No. of H-bonds	H-Bond forming Residues	The average distance of H-bonds (Å)
STAT3	5281650	α-M	−3.362	2	MET660, GLY656	2.06
STAT3	4253236	STX-0119	−2.592	2	TYR657, TYR657	2.55

Abbreviations: α-M: Alpha mangostin, STAT3: Signal Transducer and Activator of Transcription 3, MET: Methionine, GLY: Glycine, TYR: Tyrosine, STX-0119: STAT3 Inhibitor XI.

that the drug-target complexes binding energy varied. Only the most favourable position with the highest binding energy was carefully selected from the docking experiments for the inner-molecular interaction study. The docking investigation revealed that the binding energies for STAT3/α-M and STAT3/STX-0119 complexes were −3.362 and −2.592 kcal/mol, respectively. The results show that α-M has higher binding energy than STX-0119, indicating that it may have a significant anti-cancer effect than the standard inhibitor.

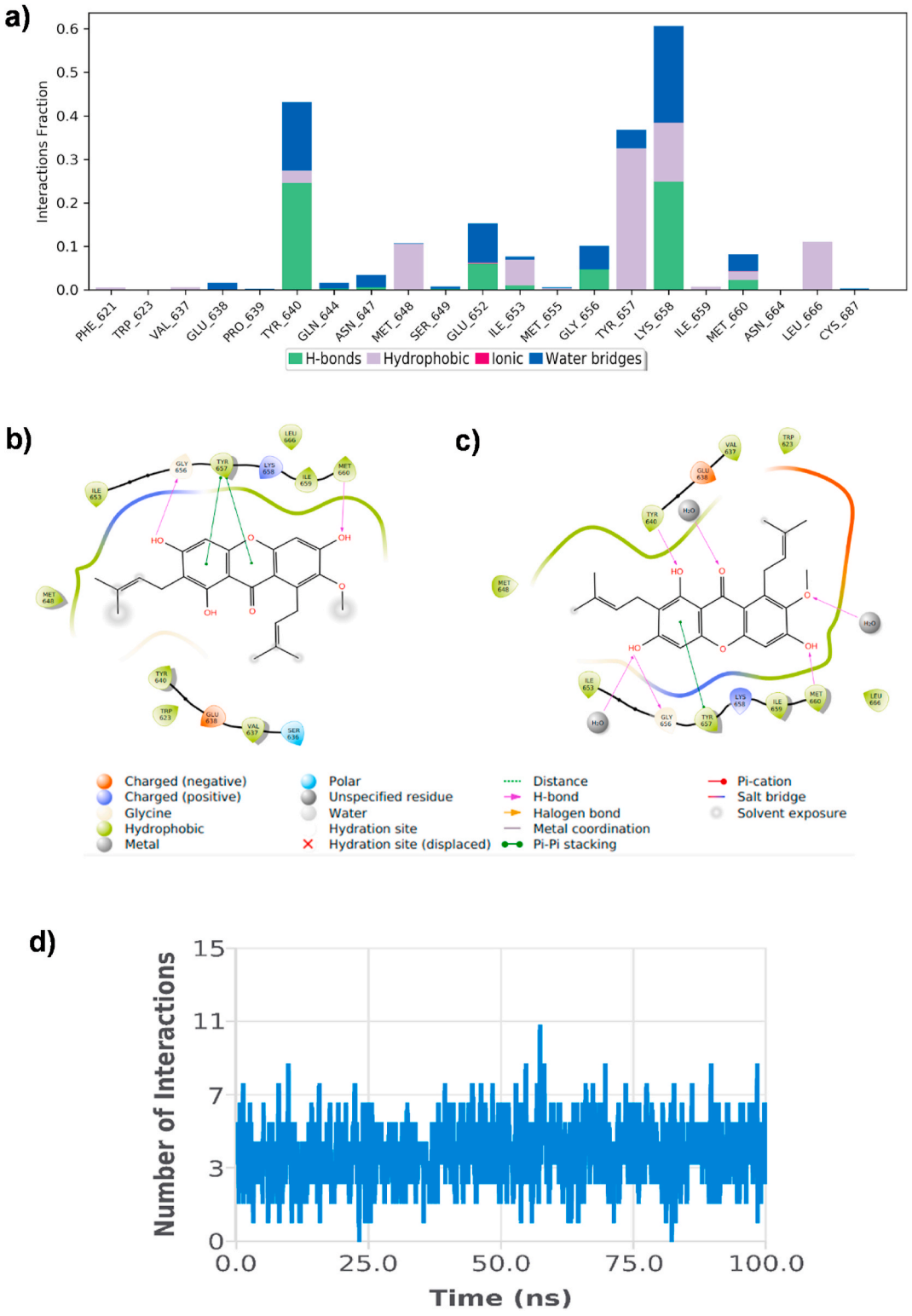

Fig. 1. Interactions of STAT3/α-M complex. a) Stacked bar chart shows protein ligand contact plot for STAT3/α-M complex during the simulation of 100 ns. Intermolecular hydrogen bonding, electrostatic and hydrophobic interactions formed between b) Pre MD STAT3/α-M complex, c) Post MD STAT3/α-M complex, d) Deviation of H-bonds contributed in interaction during 100 ns MD simulation in STAT3/α-M complex are displayed by blue lines. (For interpretation of the references to colour in this figure legend, the reader is referred to the Web version of this article.)

3.1.2. Trajectory analysis of MD simulations

The structural rearrangements of the receptor and the stability of the docked complex with α-M were evaluated using a 100 ns MD simulation. The dynamics and stability of two systems (STAT3: Apo; STAT3/α-M complex: Holo) were assessed using the Desmond suite of Schrödinger LLC, New York, NY, 2021. The RMSD profile of the backbone atoms, at 100 ns, was used to determine the dynamic stability of both systems (Apo and Holo) (Fig. S1c). Compared to the Apostate, the backbone RMSD graph of the Holo state demonstrated a stable trajectory after 80 ns of simulation. In comparison to the Holo state, which had a consistent RMSD value between 3.6 and 5.0 Å from 80 to 100 ns, the Apostate showed considerable fluctuations throughout the MD simulations (1.4–5.2 Å). This shows that α-M can stabilise protein by altering its pose. The RMSD finding was further corroborated by utilising RMSF to look at the fluctuation of residues. RMSF plots were used to observe the mobility of various residues in both phases (Fig. S1d). Overall, the Apostate had more variations than the Holo state, indicating that movement was restricted during the simulation. In the Holo state, it was discovered that amino acid residues between (40 and 80) and (260 and 300) had larger variations in their C alpha atoms than in other areas, which could be related to α-M interaction with protein. Around ten terminal residues from both the C- and N-terminal ends showed higher

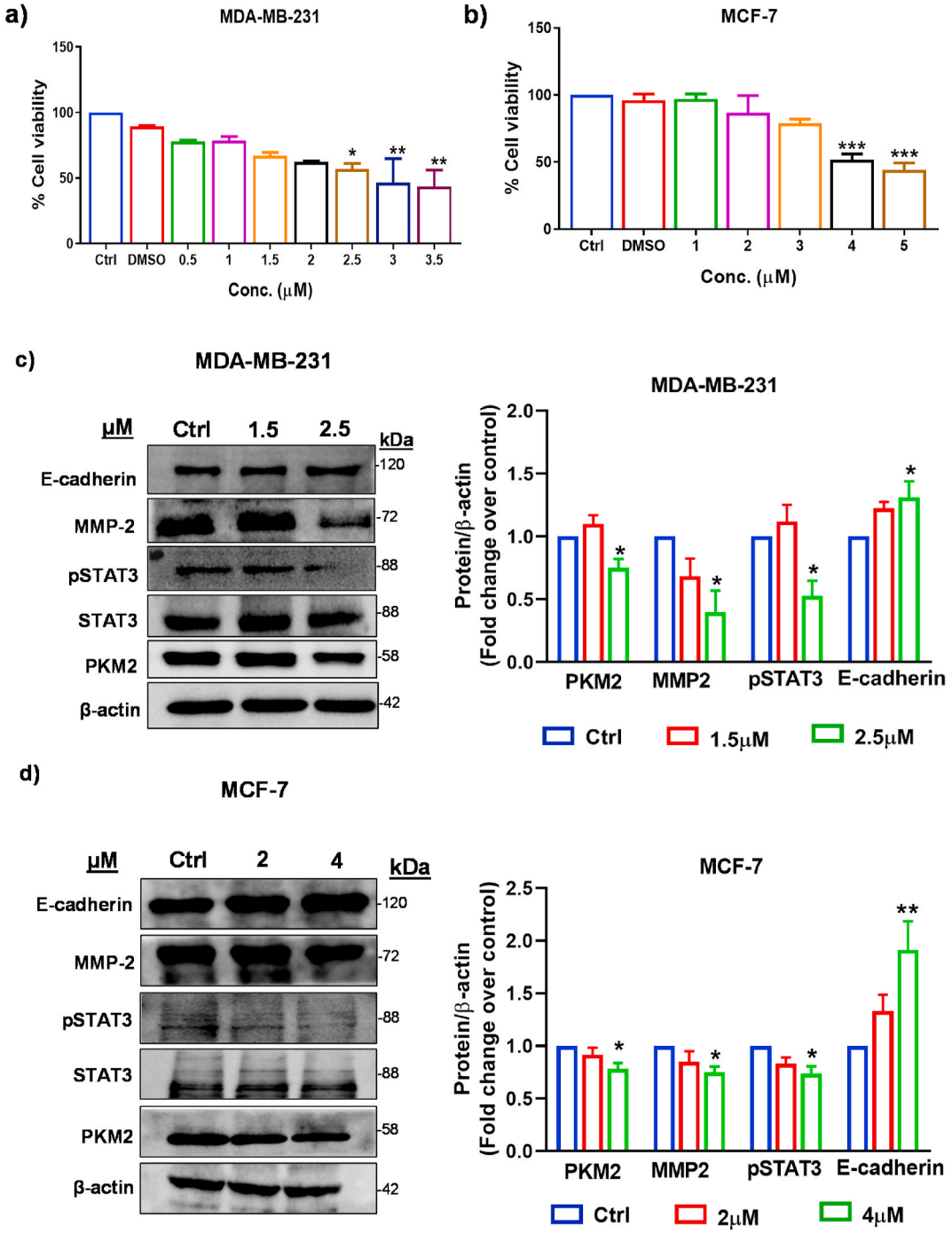

Fig. 2. α-M exhibits cytotoxicity and inhibits STAT3, PKM2, and EMT markers. α-M affects cell viability of a) MDA-MB-231 and b) MCF-7 cells. Immuno blots of pSTAT3, STAT3, PKM2, E-cadherin, and MMP2 of c) MDA-MB-231 and d) MCF-7 cells were represented after the α-M treatment. β-actin was used as a housekeeping gene. Data was expressed as mean ± SEM of three different experiments (n = 3). *p < 0.05, **p < 0.01, ***p < 0.001 significant vs. Ctrl.

variances in all states that could be overlooked. This graph shows that α-M binding reduces the mobility of residues in the Holo state compared to the Apostate. The fluctuation graphs of rGyr vs simulation (Fig. S1e) duration show that after 80 ns, rGyr remains constant over the simulation procedure. The ligand rGyr variation in the receptor-binding pocket of the protein was essentially the same, ranging from 4.2 to 4.5 and demonstrating stable behaviour of the ligand over 80ns–100ns MD simulation when compared to 1–80 ns.

SASA's illustration (Fig. S1f) states that in the Holo state, the available solvent surface was reduced. The findings of SASA revealed that the binding of α-M altered the hydrophilic and hydrophobic interaction areas, which might potentially affect the orientations in the protein surface due to the amino acid residue shift from the accessible to the buried region. During the 80ns–100ns MD simulation, the SASA graphs of the Holo state represented SASA with ~310–~470 Å.

3.1.3. H-bond analysis

During MD simulations, the intermolecular hydrogen bonds of the Holo and Apo were tracked. Throughout the simulation time, the Holo state simulation reflected a varied number of intermolecular hydrogen bonds. The stacked bar chart in Fig. 1a shows that STAT3 amino acid residues such as Tyr640, Glu652, Gly656, Lys658 and Met 660 play a crucial role in the binding and regulation of STAT3 protein. In this histogram, values over 0.39 are possible as some protein residue may make multiple contacts of the same subtype with the ligand. Corresponding to pre MD (Fig. 1b), after 100 ns of simulation, the amino acid residues Tyr640, Met660 and Gly656 were implicated in creating H-bonds with the α-M in post MD (Fig. 1c). The pre-MD STAT3/α-M complex represented two H-bonds (with an average atomic distance of 2.06 Å). Over the course of the simulation, the amount of H-bonds was directly related to the stability of the drug-target complex. The post MD analysis depicted an increase in the number of hydrogen bonding residues such as Tyr640. The residues Met660 and Gly656 did not get compensated during the course of time (Fig. 1d). This reflects attaining the potentiality against the targeted protein with time.

3.2. In-vitro study

3.2.1. α-M inhibits the viability of breast cancer cells

For determining the cytotoxicity of α-M, breast cancer cell lines (MCF-7 and MDA-MB-231) were exposed to α-M at different concentrations (0.5–5 μM) for 24 h. As shown in Fig. 2a and b, the α-M treatment showed a significant dose-dependent decrease in the cell viability. Poor migratory cell line MCF-7 tested with an IC_{50} of (***$p < 0.001$) 4 μM whereas highly invasive MDA-MB-231 cells were more sensitive to α-M treatment with IC_{50} of 2.5 μM (*$p < 0.05$). Further, we tested α-M on normal mammary epithelial cells MCF-10A and found to get no significant cytotoxicity till 5 μM (Fig. S2). So, for further studies, we used 1.5 and 2.5 μM in MDA-MB-231 and; 2 and 4 μM in MCF-7 cells. These results put forward that α-M could suppress the cell viability of breast cancer cells selectively without showing the toxicity on MCF-10A at IC_{50} concentrations. Based on these results, we investigated the mechanism of α-M on MCF-7 and MDA-MB-231 cells.

3.2.2. α-M inhibits STAT3 induced hnRNP-A1 and PKM2 expression

To understand the α-M induced cell death, we studied the phosphorylation status of STAT3, a critical signaling molecule often associated with cell survival and proliferation. Treatment of breast cancer cell lines with α-M at IC_{50} concentrations significantly inhibited the phosphorylation (Y705) of STAT3 (*$p < 0.05$) in MCF-7 and MDA-MB-231 cells (Fig. 2c and d). Further to understand the inhibitory effect of α-M on transcriptional activity of STAT3, we checked for its downstream targets. Results show that decreased pSTAT3 expression coincided with the reduced PKM2 expression (*$p < 0.05$) (Fig. 2c and d). Furthermore, as the nuclear kinase role of PKM2 is involved with metastasis, we checked the effect of α-M treatment on EMT markers like E-cadherin and MMP2. We found to have a decreased MMP-2 (*$p < 0.05$) and increased E-cadherin expression (*$p < 0.05$ in MDA-MB-231 and **$p < 0.01$ in MCF-7) significantly (Fig. 2c and d). In an attempt to understand the mechanism of downregulated PKM2 expression, we studied the mRNA levels of hnRNPA1, a splicing protein tangled in PKM gene splicing. Stimulation with α-M decreased the mRNA expression of hnRNPA1 (*$p < 0.05$, **$p < 0.01$, and ***$p < 0.001$) significantly (Fig. 3a and b). These results suggest that α-M can inhibit the PKM2 expression via regulating hnRNPA1 expression.

3.2.3. α-M inhibits the migration and invasion of breast cancer cells

As shown in (Fig. 4a and b), the results from the wound healing assay depict that α-M repressed the motility of MDA-MB-231 and MCF-7 cells (*$p < 0.05$, **$p < 0.01$, and ***$p < 0.001$). Further, with the invasion assay, we found a significant decrease (**$p < 0.01$, and ***$p < 0.001$) in the invading capacity of cancer cells (Fig. 5a and b). These results suggest that α-M stimulation induced STAT3 and PKM2 inhibition affect the invasive capability of breast cancer cells.

3.2.4. α-M treatment reduced $Ki67^+$ and $BrdU^+$ cells

Having precise results that α-M inhibited pY705 of STAT3, a cell proliferation marker, we further checked for the effect of α-M on $Ki67^+$ cells. From the results, we found that α-M treatment significantly affected the number of $Ki67^+$ cells in both MCF-7 and MDA-MB-231 (***$p < 0.001$), indicating that α-M can hinder cell proliferation by inhibiting STAT3 (Fig. 6a and b). Further, we checked the effect of α-M on BrdU incorporation in breast cancer cells. We found that α-M treatment significantly affected the BrdU incorporation in MCF-7 cells (***$p < 0.001$), whereas in MDA-MB-231, we didn't find any differences with the BrdU incorporation (Fig. 7a and b).

4. Discussion

α-M treatment decreased STAT3 induced proliferation, migration, and invasion in breast cancer cells, supporting our hypothesis. The treatment further inhibited hnRNP-A1, PKM2 and EMT markers. We discovered a significant reduction in MCF-7 and MDA-MB-231 cell migration and invasion. Furthermore, in MCF-7 we found a decrease in $Ki67^+$ and $BrdU^+$ cells, whereas in MDA-MB-231 cells we found a decrease in $Ki67^+$ but not in $BrdU^+$ cells.

Increased mortality rates among patients with metastatic breast cancer compel scientists all over the world to take the lead in developing and researching the therapeutic potential of nutraceuticals. Certain anti-metastasis drugs have advanced to clinical trials as a result of preclinical research. Several studies revealed the role of STAT3 in cancer metastasis [38,39]. As a result, there is a tremendous need to research natural coumpounds for the pharmacological intervention of STAT3. α-M is one of the most extensively researched xanthones for its anti-cancer potential [40–42]. Its inhibitory effect on STAT3-induced breast cancer progression, however, is uncertain. The current work found an link between STAT3 pY705 inhibition and alteration of downstream mediators (hnRNP-A1 and PKM2) in breast cancer progression.

For understanding the interaction between α-M and STAT3, *in-silico* docking research and MD simulations were carried out. The docking score was determined to be −3.362, indicating that the α-M and STAT3 complex had stronger affinity and stability than the conventional inhibitor (STX-0119), which exhibited −2.592. Furthermore, the dynamic stability of the docked complex with α-M was examined using a 100 ns MD simulation to predict and analyse the physical movements of atom and molecule in the context of macromolecular structure-to-function interactions [28]. The RMSD profile of the Holo state depicted aberrations for the first 80 ns and a stable trajectory after 80 ns of simulation. With Apostate, considerable fluctuations were observed throughout the MD simulation showing that α-M can stabilise the STAT3 protein. Moreover, the RMSF graph shows that α-M binding reduces the mobility of residues in the Holo state compared to the Apostate. In addition, the

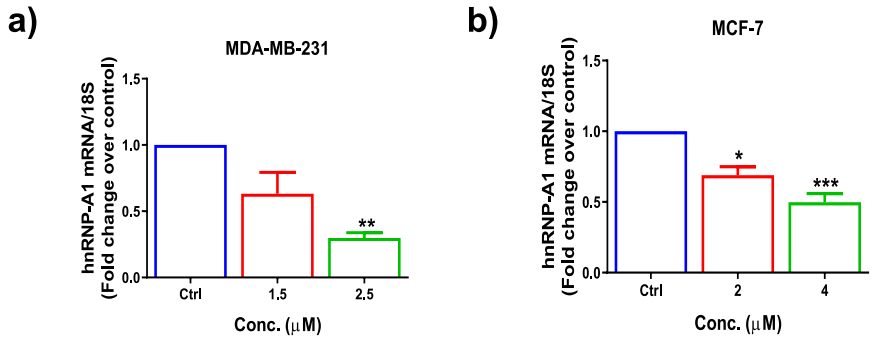

Fig. 3. α-M inhibits hnRNPA1. The mRNA expression of hnRNPA1 in a) MDA-MB-231 cells and b) MCF-7 after the α-M treatment. Data was expressed as mean ± SEM of three different experiments (n = 3). ***p < 0.001, **p < 0.01, *p < 0.05 significant vs. Ctrl.

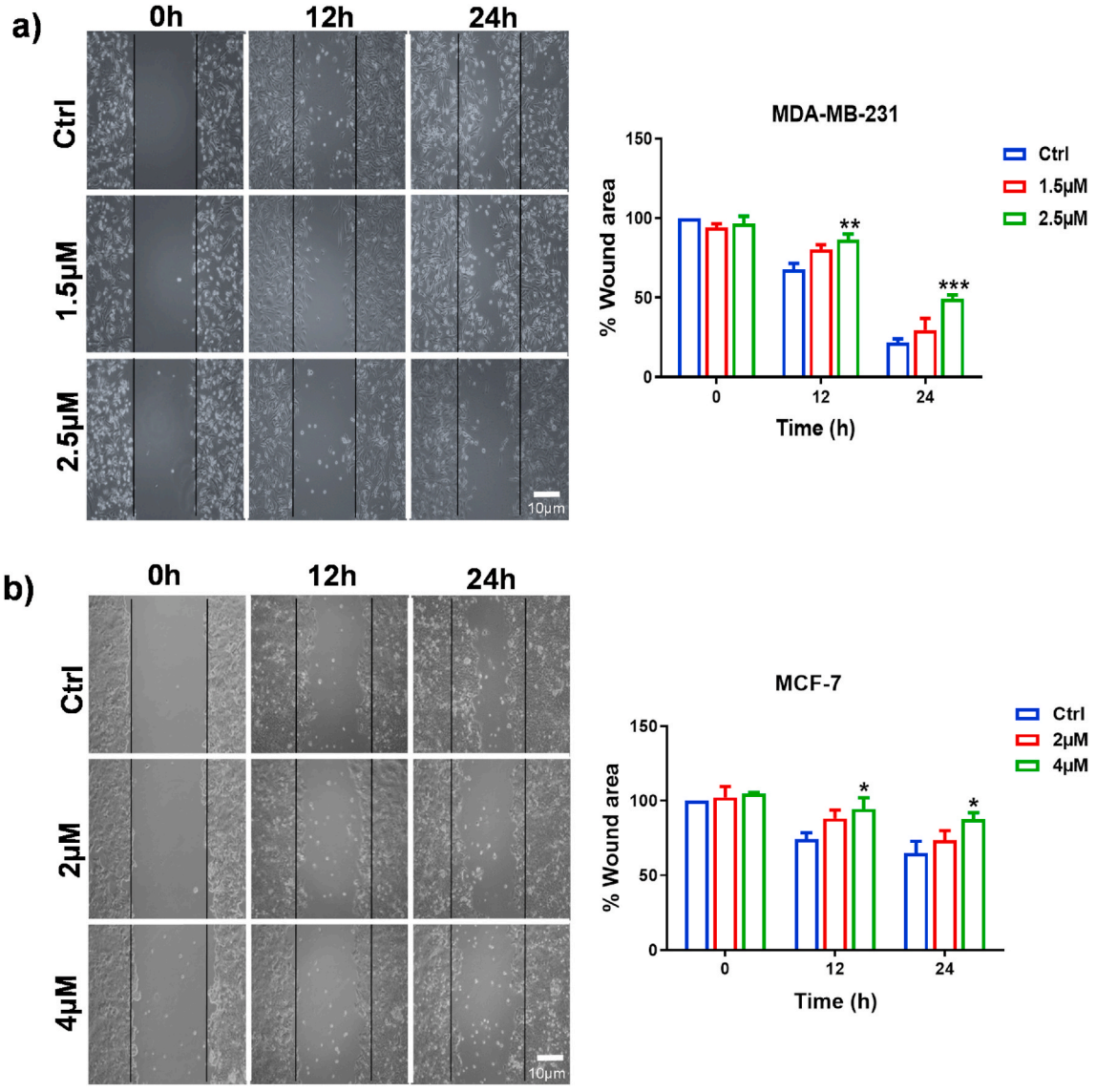

Fig. 4. α-M suppress the migration of breast cancer cells. a) Anti-migratory potential of α-M on MDA-MB-231 cells with 24 h treatment, b) Anti-migratory potential of α-M on MCF-7 cells with 24 h treatment. Representative images obtained at 0, 12, and 24 h from three different experiments (n = 3) were shown. ***p < 0.001, **p < 0.01, *p < 0.05 significant vs. Ctrl. Images were taken at 10X.

compactness for both the states and stability of α-M in the binding pocket of STAT3 receptor during the simulation of 100 ns was explained using properties such as radius of gyration (rGyr). The 'extendedness' of a ligand is measured in rGyr. The rGyr vs simulation fluctuation graphs shows that after 80 ns of simulation, the rGyr remains constant, indicating that the Holo state is more compact as the value of rGyr is

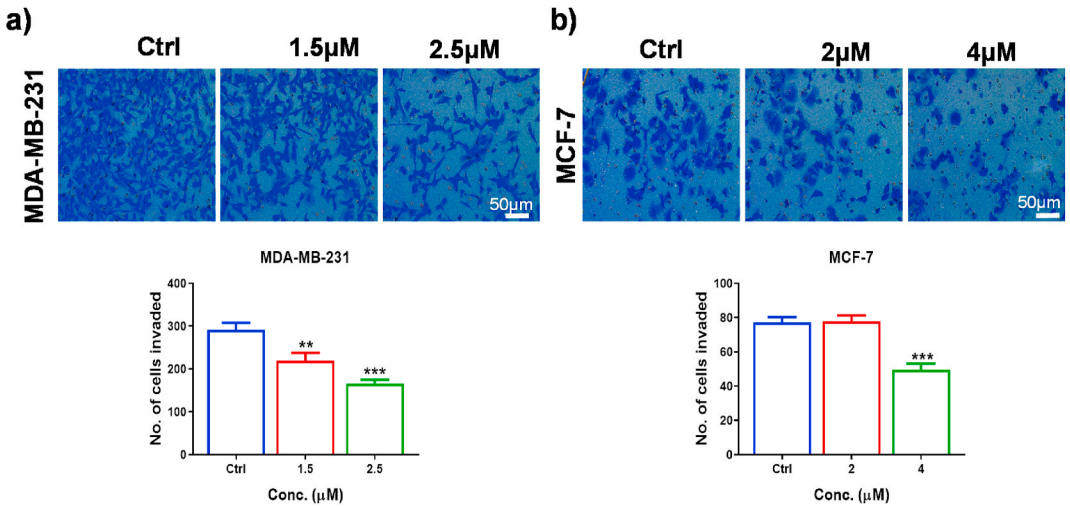

Fig. 5. α-M suppress the invasion of breast cancer cells. Treatment with α-M effected the invasiveness of a) MDA-MB-231 and b) MCF7 cells. Data was expressed as mean ± SEM and representative of three different experiments (n = 3). ***p < 0.001, **p < 0.01 significant vs. Ctrl.

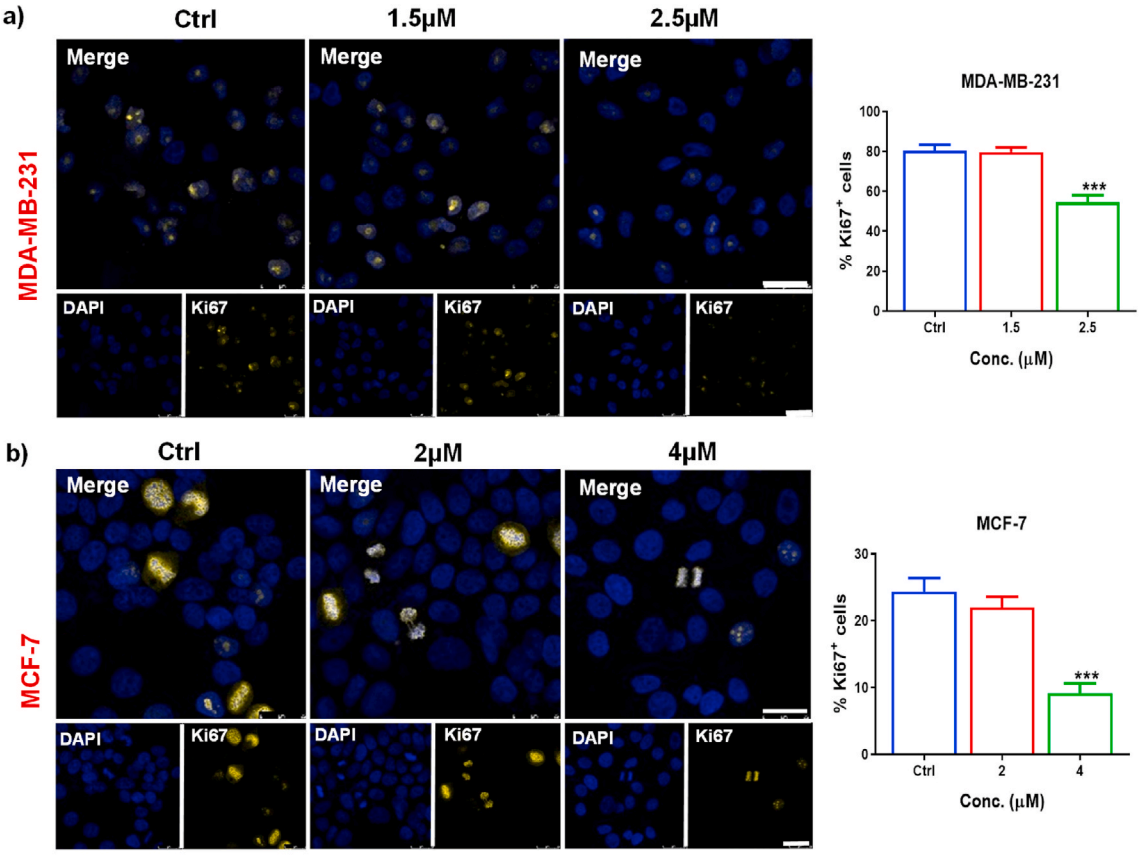

Fig. 6. α-M effects the cell proliferation of breast cancer cells affecting the levels of Ki67. Treatment with α-M affected the number of $Ki67^{+}$ cells in a) MDA-MB-231 and b) MCF-7 cells. Data was expressed as mean ± SEM and representative of three different experiments (n = 3). ***p < 0.001 significant vs. Ctrl.

inversely proportional to compactness and vice versa. These outcomes are well supported by RMSF analysis.

During simulations, amino acids are exposed to specific solvents through hydrophobic interactions. The exposed surface area is proportional to the frequency of these interactions with the solvent and the core protein residues. The findings from SASA suggests a shift of amino acid residues from access to the buried region producing an orientational change in the protein surface. Further, the interaction fraction graph tells that Tyr640, Glu652, Gly656, Lys658 and Met660 are the most critical amino acid residues in STAT3 protein for protein activity and binding. After 100 ns of simulation, we found an increase in H-bond formation with the amino acid residues Tyr640, Met660 and Gly656 in STAT3/α-M complex compared with pre-MD STAT3/α-M complex with two H-bonds. The residues Met660 and Gly656 did not get compensated over time, reflecting attaining the potentiality against the targeted protein.

As α-M has shown a strong binding activity towards STAT3 through MDS, we undertook *in-vitro* investigations to assess α-M anti-cancer

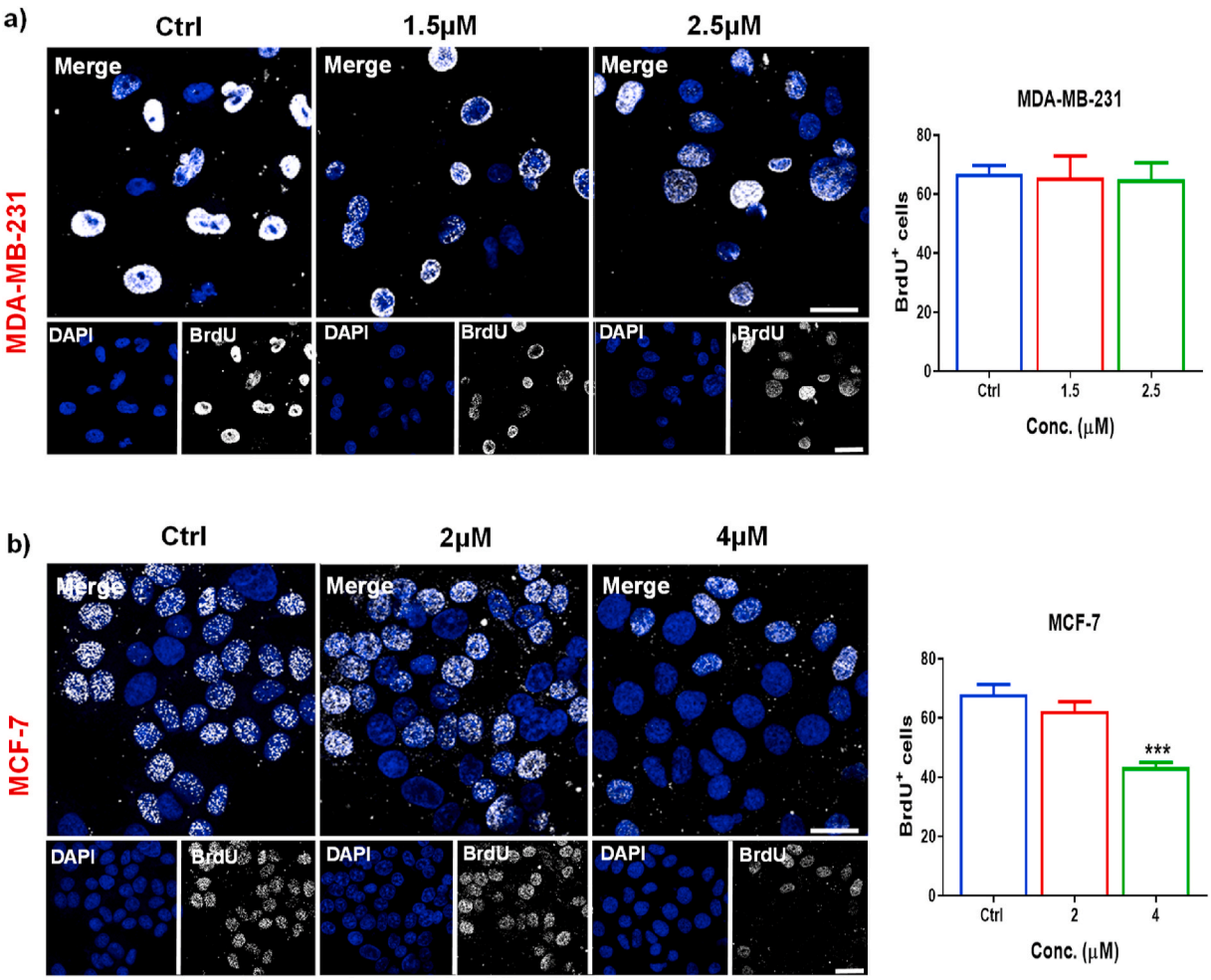

Fig. 7. α-M effects the cell proliferation of breast cancer cells affecting the levels of BrdU. Treatment with α-M affected the number of $BrdU^+$ cells in a) MDA-MB-231 and b) MCF-7 cells. Data was expressed as mean ± SEM and representative of three different experiments (n = 3). ***$p < 0.001$ significant vs. Ctrl.

potential. Following a 24 h α-M treatment, the cytotoxic test revealed cell death in MCF-7 and MDA-MB-231 cells at 4 and 2.5 μM, respectively. Interestingly, the data showed that α-M increased cell death at lower doses, indicating that cancer cells are sensitive to pharmacological treatment. The study's findings were consistent with previous research [43,44]. Furthermore, we discovered no substantial toxicity in MCF-10A cells.

STAT3 is a crucial oncogenic protein involved in cancer cell survival and proliferation. STAT3 suppression causes apoptosis, growth inhibition, and negative tumor cell invasion and treatment resistance [45]. Moreover, α-M also inhibited STAT3 against metastasis in gastric [46] and pancreatic cancer [47]. For the first time, our findings showed that α-M substantially inhibited STAT3 activity in breast cancer by decreasing its phosphorylation at tyrosine 705 residue. Yao et al. recently reported on the involvement of STAT3 in favourably regulating hnRNPA1, a splicing factor involved in the production of PKM2 protein. STAT3 interacts with the promoter area of hnRNPA1 and enhances hnRNPA1 production, which aids in splicing the PKM gene for glycolytic PKM2 protein synthesis [10,48,49]. As a result, we believe that it has the potential to interfere with hnRNP-A1 transcription. Similarly, we discovered a decrease in STAT3 activation and subsequently affecting hnRNP-A1 mRNA levels after α-M treatment. Furthermore, the current investigation demonstrated a reduction in the level of PKM2 following treatment with α-M. In summary, the findings show that α-M can indirectly influence PKM2 levels via downregulating the STAT3 pY705 levels.

The functionality of PKM2 as a protein kinase [50] positively facilitates metastasis by modulating the levels of EMT markers by regulating them at the transcriptional level [51–54]. Lentiviral PKM2 knockdown inhibited cell migration and invasion in ovarian cancer by increasing cell-cell adhesion molecules like E-cadherin and decreasing matrix metalloproteases like MMP-2 and MMP-9 [55,56]. To validate this, we used a wound-healing experiment and an invasion assay to examine the effect of α-M on PKM2-mediated cell migration and invasion. After 24 h of treatment, α-M substantially reduced the migration and invasion of MCF-7 and MDA-MB-231 cells compared to control. Furthermore, immunoblotting results revealed a considerable rise in E-cadherin and a decrease in MMP-2 levels, indicating α-M's anti migratory efficacy. A recent study also confirmed that the transcriptional control of cyclinD1 by STAT3 is needed for metastasis [57]. Furthermore, α-M was discovered to be anti-metastatic and anti-apoptotic by adversely influencing MMP levels by blocking the tRXR/Akt/cyclin D1 axis [58], hinting that STAT3 may have the crosstalk with other signalling molecules to inhibit metastasis. In addition, we looked at Ki67 and BrdU cell proliferation markers. The immunofluorescence data show that α-M considerably influenced Ki67 positive cells in MCF-7 and MDA-MB-231 cells, but α-M treatment significantly affected BrdU incorporation in MCF-7 but not in MDA-MB-231 cells. These findings support the anti-proliferative action of α-M. This study has some limitations: 1) The lack of *in-vivo* study, 2) Lack of knockdown studies to exactly validate the role of STAT3 in downregulating the downstream targets.

5. Conclusion

The current study has explored the association between STAT3 phosphorylation with hnRNP-A1 and PKM2 levels. Based on our results, we can conclude that α-M can impede breast cancer cells' invasive capability and proliferative capacity. Our study adds a new therapeutic target for α-M in breast cancer and encourages the researchers to sightsee this compound further.

Author declarations

The authors reported no potential conflict of interest.

Funding

This supplement was supported by the seed fund of the National Institute of Pharmaceutical Education and Research (NIPER)-Ahmedabad, Department of Pharmaceutics, Ministry of Chemicals and Fertilizers, Government of India. Dr Amit Khairnar gratefully acknowledges the support of the Ramalingaswami fellowship (No. BT/RLF/Re-entry/24/2017) from the Department of Biotechnology. They are supported by project no. LX22NPO5107 (MEYS): financed by European Union – Next Generation EU.

Author's contribution

The authors' contributions are as follows: **Lakshmi Vineela Nalla:** Conceptualization; Data curation; Formal analysis, Investigation; Methodology; Software; Validation; Roles/Writing - original draft; Writing - review and editing, **Anil Dharavath:** Data curation; Formal analysis, **Santosh Kumar Behera:** Data curation of *in-silico* studies; Writing - review and editing, **Amit Khairnar:** Conceptualization; Project administration; Resources; Funding acquisition; Visualization; Writing - review and editing.

Declaration of competing interest

The authors declare that they have no known competing financial interests or personal relationships that could have appeared to influence the work reported in this paper.

Acknowledgement

The authors acknowledge Ms. Monika Seervi for the imaging studies.

Appendix A. Supplementary data

Supplementary data to this article can be found online at https://doi.org/10.1016/j.adcanc.2023.100089.

References

[1] B.P. George, R. Chandran, H. Abrahamse, Role of phytochemicals in cancer chemoprevention: insights, Antioxidants 10 (9) (2021) 1455.
[2] A.B. Mariotto, R. Etzioni, M. Hurlbert, L. Penberthy, M. Mayer, Estimation of the number of women living with metastatic breast cancer in the United States, Cancer Epidemiology and Prevention Biomarkers 26 (6) (2017) 809–815.
[3] R.L. Siegel, K.D. Miller, A. Jemal, Cancer statistics, CA A Cancer J. Clin. 69 (1) (2019) 7–34, 2019.
[4] H. Sung, J. Ferlay, R.L. Siegel, M. Laversanne, I. Soerjomataram, A. Jemal, et al., Global cancer statistics 2020: GLOBOCAN estimates of incidence and mortality worldwide for 36 cancers in 185 countries, CA A Cancer J. Clin. 71 (3) (2021) 209–249.
[5] I. Gkouveris, N. Nikitakis, J. Sauk, STAT3 signaling in cancer, J. Cancer Ther. 6 (2015) 709, 08.
[6] L.V. Nalla, K. Kalia, A. Khairnar, Self-renewal signaling pathways in breast cancer stem cells, Int. J. Biochem. Cell Biol. 107 (2019) 140–153.
[7] J.P. Couto, L. Daly, A. Almeida, J.A. Knauf, J.A. Fagin, M. Sobrinho-Simões, et al., STAT3 negatively regulates thyroid tumorigenesis, Proc. Natl. Acad. Sci. USA 109 (35) (2012) E2361–E2370.
[8] H.M. Amin, T.J. McDonnell, Y. Ma, Q. Lin, Y. Fujio, K. Kunisada, et al., Selective inhibition of STAT3 induces apoptosis and G(1) cell cycle arrest in ALK-positive anaplastic large cell lymphoma, Oncogene 23 (32) (2004) 5426–5434.
[9] F. Zhang, C. Li, H. Halfter, J. Liu, Delineating an oncostatin M-activated STAT3 signaling pathway that coordinates the expression of genes involved in cell cycle regulation and extracellular matrix deposition of MCF-7 cells, Oncogene 22 (6) (2003) 894–905.
[10] A. Yao, Y. Xiang, Y.R. Si, L.J. Fan, J.P. Li, H. Li, et al., PKM2 promotes glucose metabolism through a let-7a-5p/Stat3/hnRNP-A1 regulatory feedback loop in breast cancer cells, J. Cell. Biochem. 120 (4) (2019) 6542–6554.
[11] W. Qin, Y. Tian, J. Zhang, W. Liu, Q. Zhou, S. Hu, et al., The double inhibition of PDK1 and STAT3-Y705 prevents liver metastasis in colorectal cancer, Sci. Rep. 9 (1) (2019) 1–12.
[12] A. Wong, R.A. Soo, D. Tan, S.C. Lee, J. Lim, P. Marban, et al., Phase I and biomarker study of OPB-51602, a novel signal transducer and activator of transcription (STAT) 3 inhibitor, in patients with refractory solid malignancies, Ann. Oncol. 26 (5) (2015) 998–1005.
[13] K-j Zhang, Q-l Gu, K. Yang, X-j Ming, J-x Wang, Anticarcinogenic effects of α-mangostin: a review, Planta Med. 83 (2017) 188–202, 03/04.
[14] S.C. Gupta, A.B. Kunnumakkara, S. Aggarwal, B.B. Aggarwal, Inflammation, a double-edge sword for cancer and other age-related diseases, Front. Immunol. 9 (2018).
[15] P. Li, W. Tian, X. Ma, Alpha-mangostin inhibits intracellular fatty acid synthase and induces apoptosis in breast cancer cells, Mol. Cancer 13 (1) (2014) 1–11.
[16] I. Bissoli, C. Muscari, Doxorubicin and α-Mangostin oppositely affect luminal breast cancer cell stemness evaluated by a new retinaldehyde-dependent ALDH assay in MCF-7 tumor spheroids, Biomed. Pharmacother. 124 (2020), 109927.
[17] T.K.T. Phan, F. Shahbazzadeh, T.T.H. Pham, T. Kihara, Alpha-mangostin inhibits the migration and invasion of A549 lung cancer cells, PeerJ 6 (2018), e5027.
[18] C.-M. Chen, S.-C. Hsieh, C.-L. Lin, Y.-S. Lin, J.-P. Tsai, Y.-H. Hsieh, Alpha-mangostin suppresses the metastasis of human renal carcinoma cells by targeting MEK/ERK expression and MMP-9 transcription activity, Cell. Physiol. Biochem. 44 (4) (2017) 1460–1470.
[19] S. Beninati, S. Oliverio, M. Cordella, S. Rossi, C. Senatore, I. Liguori, et al., Inhibition of cell proliferation, migration and invasion of B16-F10 melanoma cells by α-mangostin, Biochem. Biophys. Res. Commun. 450 (4) (2014) 1512–1517.
[20] H. Jiang, N. Ma, Y. Shang, W. Zhou, T. Chen, D. Guan, et al., Triosephosphate isomerase 1 suppresses growth, migration and invasion of hepatocellular carcinoma cells, Biochem. Biophys. Res. Commun. 482 (4) (2017) 1048–1053.
[21] S.-H. Hung, K.-H. Shen, C.-H. Wu, C.-L. Liu, Y.-W. Shih, α-Mangostin suppresses PC-3 human prostate carcinoma cell metastasis by inhibiting matrix metalloproteinase-2/9 and urokinase-plasminogen expression through the JNK signaling pathway, J. Agric. Food Chem. 57 (4) (2009) 1291–1298.
[22] Q. Xu, J. Ma, J. Lei, W. Duan, L. Sheng, X. Chen, et al., -Mangostin suppresses the viability and epithelial-mesenchymal transition of pancreatic cancer cells by downregulating the PI3K/akt pathway, BioMed Res. Int. 2014 (2014).
[23] R. Tang, C. Yang, X. Ma, Y. Wang, D. Luo, C. Huang, et al., MiR-let-7a inhibits cell proliferation, migration, and invasion by down-regulating PKM2 in gastric cancer, Oncotarget 7 (5) (2016) 5972.
[24] R. Fu, P. Yang, S. Amin, Z. Li, A novel miR-206/hnRNPA1/PKM2 axis reshapes the Warburg effect to suppress colon cancer growth, Biochem. Biophys. Res. Commun. 531 (4) (2020) 465–471.
[25] E.P. Glide, Docking and scoring incorporating a model of hydrophobic enclosure for protein-ligand complexes, J. Med. Chem. 4 (2006) 6177–6196.
[26] H.-T. Li, X. Zhu, Quinoline-based compounds with potential activity against drugresistant cancers, Curr. Top. Med. Chem. 21 (5) (2021) 426–437.
[27] S.K. Behera, N. Vhora, D. Contractor, A. Shard, D. Kumar, K. Kalia, et al., Computational drug repurposing study elucidating simultaneous inhibition of entry and replication of novel corona virus by Grazoprevir, Sci. Rep. 11 (1) (2021) 1–11.
[28] J.D. Durrant, J.A. McCammon, Molecular dynamics simulations and drug discovery, BMC Biol. 9 (1) (2011) 1–9.
[29] R. Raghu, V. Devaraji, K. Leena, S. Riyaz, P. Baby Rani, P. Kumar Naik, et al., Virtual screening and discovery of novel aurora kinase inhibitors, Curr. Top. Med. Chem. 14 (17) (2014) 2006–2019.
[30] D. Shivakumar, J. Williams, Y. Wu, W. Damm, J. Shelley, W. Sherman, Prediction of absolute solvation free energies using molecular dynamics free energy perturbation and the OPLS force field, J. Chem. Theor. Comput. 6 (5) (2010) 1509–1519.
[31] I. Aier, P.K. Varadwaj, U. Raj, Structural insights into conformational stability of both wild-type and mutant EZH2 receptor, Sci. Rep. 6 (1) (2016) 1–10.
[32] U. Deniz, E. Ozkirimli, K.O. Ulgen, A systematic methodology for large scale compound screening: a case study on the discovery of novel S1PL inhibitors, J. Mol. Graph. Model. 63 (2016) 110–124.
[33] A. Parkhe, P. Parekh, L.V. Nalla, N. Sharma, M. Sharma, A. Gadepalli, et al., Protective effect of alpha mangostin on rotenone induced toxicity in rat model of Parkinson's disease, Neurosci. Lett. (2019), 134652.
[34] L.V. Nalla, P. Gondaliya, K. Kalia, A. Khairnar, Targeting specificity protein 1 with miR-128-3p overcomes TGF-β1 mediated epithelial-mesenchymal transition in breast cancer: an in vitro study, Mol. Biol. Rep. (2022) 1–10.
[35] Y. Ning, C. Wang, X. Liu, Y. Du, S. Liu, K. Liu, et al., CK2-mediated CCDC106 phosphorylation is required for p53 degradation in cancer progression, J. Exp. Clin. Cancer Res. 38 (1) (2019) 131.
[36] J. Pijuan, C. Barceló, D.F. Moreno, O. Maiques, P. Sisó, R.M. Marti, et al., In vitro cell migration, invasion, and adhesion assays: from cell imaging to data analysis, Front. Cell Dev. Biol. 7 (2019) 107.

[37] Abcam, Available from: https://www.abcam.com/protocols/brdu-staining-protocol. (Accessed 16 July 2021) https://www.abcam.com/protocols/brdu-staining-protocol.
[38] M.Z. Kamran, P. Patil, R.P. Gude, Role of STAT3 in cancer metastasis and translational advances, BioMed Res. Int. 2013 (2013).
[39] S.N.R. Gajula, D.N.J. Bale, S.K. Nanjappan, Analytical and omics approaches in the identification of oxidative stress-induced cancer biomarkers, Handbook of Oxidative Stress in Cancer: Mechanistic Aspects-Springer (2020) 1–24.
[40] B. Wudtiwai, P. Pitchakarn, R. Banjerdpongchai, Alpha-mangostin, an active compound in Garcinia mangostana, abrogates anoikis-resistance in human hepatocellular carcinoma cells, Toxicol. Vitro 53 (2018) 222–232.
[41] G. Scolamiero, C. Pazzini, F. Bonafè, C. Guarnieri, C. Muscari, Effects of α-mangostin on viability, growth and cohesion of multicellular spheroids derived from human breast cancer cell lines, Int. J. Med. Sci. 15 (1) (2018) 23.
[42] C.-H. Lee, T.-H. Ying, H.-L. Chiou, S.-C. Hsieh, S.-H. Wen, R.-H. Chou, et al., Alpha-mangostin induces apoptosis through activation of reactive oxygen species and ASK1/p38 signaling pathway in cervical cancer cells, Oncotarget 8 (29) (2017), 47425.
[43] P. Li, W. Tian, X. Ma, Alpha-mangostin inhibits intracellular fatty acid synthase and induces apoptosis in breast cancer cells, Mol. Cancer 13 (1) (2014) 138.
[44] W. Huang, Y. Liang, X. Ma, Alpha-mangostin induces endoplasmic reticulum stress and autophagy which count against fatty acid synthase inhibition mediated apoptosis in human breast cancer cells, Cancer Cell Int. 19 (1) (2019) 151.
[45] A.L. Wong, J.L. Hirpara, S. Pervaiz, J.-Q. Eu, G. Sethi, B.-C. Goh, Do STAT3 inhibitors have potential in the future for cancer therapy? Expet Opin. Invest. Drugs 26 (8) (2017) 883–887.
[46] T. Shan, X-j Cui, W. Li, W-r Lin, H-w Lu, Y-m Li, et al., α-Mangostin suppresses human gastric adenocarcinoma cells in vitro via blockade of Stat3 signaling pathway, Acta Pharmacol. Sin. 35 (8) (2014) 1065.
[47] B.B. Hafeez, A. Mustafa, J.W. Fischer, A. Singh, W. Zhong, M.O. Shekhani, et al., α-Mangostin: a dietary antioxidant derived from the pericarp of Garcinia mangostana L. inhibits pancreatic tumor growth in xenograft mouse model, Antioxidants Redox Signal. 21 (5) (2014) 682–699.
[48] C.J. David, M. Chen, M. Assanah, P. Canoll, J.L. Manley, HnRNP proteins controlled by c-Myc deregulate pyruvate kinase mRNA splicing in cancer, Nature 463 (7279) (2010) 364.
[49] C.V. Clower, D. Chatterjee, Z. Wang, L.C. Cantley, M.G. Vander Heiden, A. R. Krainer, The alternative splicing repressors hnRNP A1/A2 and PTB influence pyruvate kinase isoform expression and cell metabolism, Proc. Natl. Acad. Sci. USA 107 (5) (2010) 1894–1899.
[50] M. Rihan, L.V. Nalla, A. Dharavath, S. Patel, A. Shard, A.J.B. Khairnar, et al., Boronic Acid Derivative Activates Pyruvate Kinase M2 Indispensable for Redox Metabolism in Oral Cancer Cells, 2022, 128539.
[51] T.-Y. Cheng, Y.-C. Yang, H.-P. Wang, Y.-W. Tien, C.-T. Shun, H.-Y. Huang, et al., Pyruvate kinase M2 promotes pancreatic ductal adenocarcinoma invasion and metastasis through phosphorylation and stabilization of PAK2 protein, Oncogene 37 (13) (2018) 1730.
[52] Y. Lin, F. Meng, Z. Lu, K. Chen, Y. Tao, Y. Ouyang, et al., Knockdown of PKM2 suppresses tumor progression in human cervical cancer by modulating epithelial–mesenchymal transition via Wnt/β-catenin signaling, Cancer Manag. Res. 10 (2018) 4191.
[53] W. Wang, Q. He, J. Sun, Z. Liu, L. Zhao, Z. Lu, et al., Pyruvate kinase M2 deregulation enhances the metastatic potential of tongue squamous cell carcinoma, Oncotarget 8 (40) (2017), 68252.
[54] A. Hamabe, M. Konno, N. Tanuma, H. Shima, K. Tsunekuni, K. Kawamoto, et al., Role of pyruvate kinase M2 in transcriptional regulation leading to epithelial–mesenchymal transition, Proc. Natl. Acad. Sci. USA 111 (43) (2014) 15526–15531.
[55] Y. Miao, M. Lu, Q. Yan, S. Li, Y. Feng, Inhibition of proliferation, migration, and invasion by knockdown of pyruvate kinase-M2 (PKM2) in ovarian cancer SKOV3 and OVCAR3 cells, Oncol. Res. 24 (6) (2016) 463–475.
[56] L.-Y. Wang, Y.-P. Liu, L.-G. Chen, Y.-L. Chen, L. Tan, J.-J. Liu, et al., Pyruvate kinase M2 plays a dual role on regulation of the EGF/EGFR signaling via E-cadherin-dependent manner in gastric cancer cells, PLoS One 8 (6) (2013), e67542.
[57] J. Luo, R. Yan, X. He, J. He, Constitutive activation of STAT3 and cyclin D1 overexpression contribute to proliferation, migration and invasion in gastric cancer cells, Am. J. Tourism Res. 9 (12) (2017) 5671.
[58] X. Zhu, J. Li, H. Ning, Z. Yuan, Y. Zhong, S. Wu, et al., α-Mangostin induces apoptosis and inhibits metastasis of breast cancer cells via regulating rxrα-AKT signaling pathway, Front. Pharmacol. 12 (2021), 739658, https://doi.org/10.3389/fphar.2021.739658.